Journal of Electron Microscopy **0(0)**: 1–8 (2011)
doi: 10.1093/jmicro/dfr015

Physical: Full-length

Electron holography study of remanence states in exchange-biased MnPd/Fe bilayers grown epitaxially on MgO(001)

Jong Seok Jeong[1,*], Zentaro Akase[1], Daisuke Shindo[1], Qing-feng Zhan[2] and Kannan M. Krishnan[2]

[1]Institute of Multidisciplinary Research for Advanced Materials, Tohoku University, Sendai 980-8577, Japan and [2]Materials Science and Engineering, University of Washington, Seattle, WA 98195, USA
*To whom correspondence should be addressed. E-mail: jsjeong@tagen.tohoku.ac.jp

Abstract We investigated magnetic remanence states of epitaxially grown, exchange-biased MnPd/Fe bilayers by electron holography emphasizing the crystallographic orientations of the layers. Thin-foil transmission electron microscopy (TEM) specimens were carefully prepared along both hard and easy axes of the Fe layer. The *ex situ* magnetization-reversal process was carried out using the TEM specimens, and magnetic flux densities of the ultra-thin Fe layers were evaluated at different remanence states. We show that a spin configuration in the TEM specimens is determined by the competition between an exchange coupling at the MnPd/Fe bilayer interface, shape anisotropy of TEM specimens and intrinsic magnetocrystalline anisotropy of Fe.

Keywords electron holography, demagnetizing effects, shape anisotropy, magnetic flux density, exchange bias, TEM

Received 20 January 2011, accepted 9 March 2011

Introduction

Exchange bias (EB) is a shift in the magnetic hysteresis loop by a coupling at the interface between an antiferromagnetic (AFM) and a ferromagnetic (FM) material [1]. Since the discovery [1] of the EB effect in 1956, a number of EB systems, such as layered thin-film structures, small particles, inhomogeneous materials and coated AFM single crystals [1–4], have been investigated using many experimental techniques [5–8]. Nevertheless, a complete theoretical understanding of EB has been elusive [9–13]. The difficulty in establishing a uniformly acceptable theory/model of EB is largely due to inadequate characterization of the AFM–FM interface on an atomic scale. Recent transmission electron microscopy (TEM) investigations have made it possible to visualize structural and chemical information on an atomic level, and insights into the physical and magnetic microstructures of exchange-biased spin valves and related system were provided using several TEM techniques including high-resolution TEM and Lorentz electron microscopy [14–16]. Electron holography also is a powerful technique that can investigate the magnetic structure in FM materials by analyzing the phase shift of electrons in TEM [17] although AFM materials cannot be analyzed because they have no magnetization that can shift the phase of the electrons. To date, electron holography has been applied to the study of the magnetization-reversal mechanisms and remanence states in exchange-biased CoFe/FeMn patterned nanostructures using plan-view specimens [18]. However, the interfacial properties and the spin-coupling between AFM and FM materials have not been investigated by electron holography using cross-sectional specimens with an

ultra-thin FM film. In addition, electron holography, based on TEM using thin-foil specimens, inevitably accompanies the effect of shape anisotropies due to geometry of the TEM specimen [19]. In order to apply electron holography to the interfacial characterization of EB systems, it is, therefore, also necessary to investigate the effects of the shape anisotropies for retrieving intrinsic interfacial properties of the EB systems from the results obtained using electron holography.

In this paper, electron holography was applied to investigate the spin configurations at the AFM–FM interface in an epitaxial, MnPd/Fe, bilayer system exhibiting EB using cross-sectional TEM specimens. In order to effectively control and characterize the interfacial structure and spin configuration, epitaxially grown MnPd/Fe thin films with well-controlled crystallographic orientations were chosen. The magnetization-reversal process was conducted along hard and easy axes of a Fe layer, and magnetic flux densities at different remanence states were estimated. In addition, the spin-configuration scheme of the MnPd/Fe bilayers in TEM specimens was *quantitatively* resolved considering the shape anisotropies of the TEM specimens.

Methods

Two types of epitaxially grown thin-film samples with a layer sequence of Pt(4 nm)/MnPd(30 nm)/Fe (8 nm)/MgO(001) were prepared by an ultrahigh vacuum ion-beam sputter deposition according to crystallographic orientation relationships between a MnPd layer and a MgO substrate, i.e. the samples with *c*- and *a*-oriented MnPd on the MgO substrate [20,21]. The structural property of the MnPd layer can be controlled by varying the substrate temperature during growth; as the temperature increases from below 100°C to above 450°C, the crystallographic orientation of the MnPd layer varies from a twinned *a*-axis to a single-crystalline *c*-axis orientation with respect to the normal of the substrate. The epitaxial relationships between the layers and the substrate are MnPd(001)//Fe(001)//MgO(001) and MnPd[100]//Fe[110]//MgO[100] for the *c*-oriented sample (Fig. 1a and c) and a bicrystal orientation with the possibility of exhibiting a twinned crystal structure for the *a*-oriented sample (Fig. 1b and d).

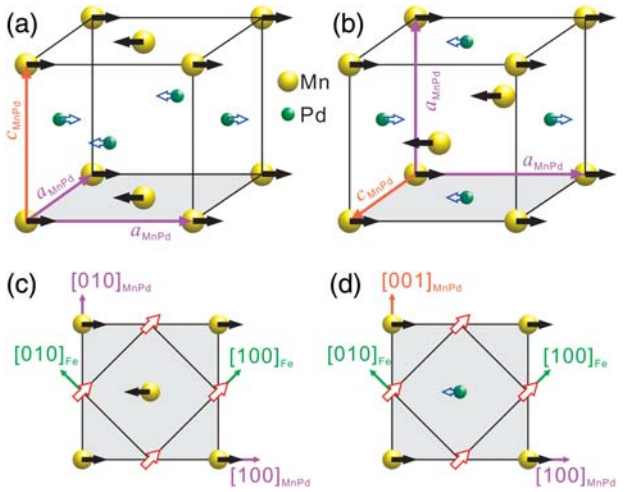

Fig. 1. Schematic illustration of a magnetic structure and interface spin configurations of MnPd according to its crystallographic orientations; (a, c) *c*-oriented and (b, d) *a*-oriented MnPd on the substrate. The interface spin configurations of MnPd in the bottom (gray-colored) of the unit cell and the crystallographic orientation relationship with Fe are presented at (c) and (d), where the spins from Pd (small open arrow), Mn (solid arrow) and Fe (big open arrow) are presented. The Mn spins are compensated for the *c*-oriented MnPd, while they are uncompensated for the *a*-oriented one.

At room temperature (RT), it is known [22] that MnPd with a CuAu–I structure has a type B magnetic structure with magnetic moments of Mn parallel to <100> and a very small contribution from Pd parallel to <100>. Figure 1 shows the magnetic structure of MnPd, the crystallographic orientation relationship between MnPd and Fe and the interface spin configurations in the two different samples. At the terminating layer, indicated by gray color in Fig. 1, of an ideal interface between MnPd and Fe, a Mn spin-lattice for the *c*-oriented MnPd is compensated (Fig. 1c), whereas for an *a*-oriented MnPd, it is spin-uncompensated (Fig. 1d). All samples were grown in the presence of an in-plane magnetic field of 300 Oe along the [100]-direction of Fe (bias direction).

For electron holographic studies, electron-transparent specimens of both *c*- and *a*-oriented samples were elaborately prepared along the hard- and easy-axis directions of the Fe layer using a focused ion beam (FIB) (JEOL, JIB-4500), as illustrated in Fig. 2a and b. Here, the TEM specimens along the hard axis for the *c*- and *a*-oriented samples are denoted as ***c*-H** and ***a*-H**, and the specimens along the easy axis for the *c*- and *a*-oriented samples are denoted as ***c*-E** and ***a*-E**. The thickness of the specimens, which includes damaged layers

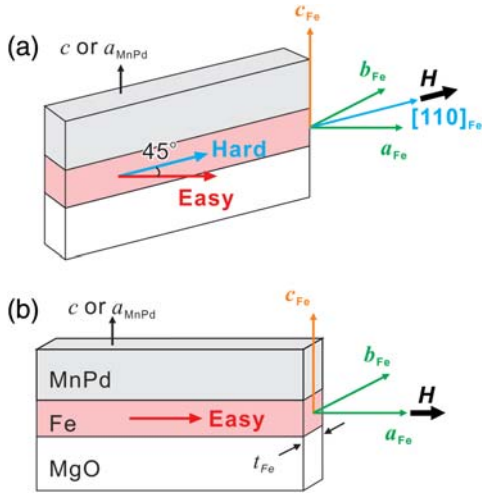

Fig. 2. Orientations in cross-sectional TEM specimens prepared along (a) hard and (b) easy axes of Fe layers. Applied field (H) direction for the magnetization-reversal process is presented.

of about 15 nm in surfaces due to FIB milling, was estimated using electron energy-loss spectroscopy (EELS) with a Gatan imaging filter.

Magnetic hysteresis curves of thin-film samples along both hard and easy axes of the Fe layer were obtained using the magneto-optical Kerr effect (MOKE) at RT. In addition, to investigate different remanence states using electron holography, the magnetization-reversal process was carried out using external magnetic field (H) of ~1500 Oe outside TEM along the direction parallel to layer interfaces and the in-plane of the TEM specimens, as shown in Fig. 2, i.e. ***c*-H** and ***a*-H** were magnetized along the Fe hard axis, while ***c*-E** and ***a*-E** were magnetized along the Fe easy axis. The magnetization-reversal process was twice conducted to confirm reproducibility of the evaluation of the magnetization. Accordingly, five different remanence states, namely as-grown state (R_{as}) and descending (R_{d1} and R_{d2}) and ascending (R_{a1} and R_{a2}) states in hysteresis loop, were investigated for four types of TEM specimens (***c*-H**, ***a*-H**, ***c*-E** and ***a*-E**).

Electron holography experiments, with a biprism voltage of 40 V, were carried out in a JEOL JEM-3000F TEM installed with a field emission gun, a biprism and a special objective lens fitted with a magnetic shield. The reconstructed phase images are presented in terms of the cosine of the phase (ϕ) and amplified with a factor of 10 in this work.

The phase image reconstructed from an electron hologram contains not only information on a magnetic field, but also that on an electrical mean inner potential. The latter can result in significant spatial variations in electron holography results, especially when the specimen thickness changes abruptly. Even though a thickness variation in the TEM specimen prepared by FIB is not considerable, an effect of the mean inner potential can be a serious obstacle for analyzing the magnetic field in the sample consisting of ultra-thin layers, such as the Fe layer in this experiment. In order to precisely investigate a true magnetic signal of the Fe layers, therefore, it is necessary to separate the electrical contribution from the magnetic one. In this experiment, the effect of the mean inner potential was eliminated using a simple time-reversal operation of an electron beam, proposed by Tonomura *et al.* [23]. A pair of holograms is obtained by observing the same specimen with the electron beam incident in two directions: upward and downward with respect to the specimen. Since the mean inner potential is a scalar and not a vector, it can be canceled out by subtracting one of these images from the other. Figure 3 shows an electron hologram and reconstructed phase images with/without the effect of the mean inner potential, obtained from ***c*-H**. Before eliminating the effect, a phase image was conventionally reconstructed from the hologram of Fig. 3a (Fig. 3b). It shows strong fringes at the edge of the specimen and at the interface of various layers as indicated by the arrows in Fig. 3b. It means that the reconstructed phase image includes the effect of the mean inner potential by abrupt thickness changes at the end of the specimen (black arrow) and the thickness variation and different material property between C and Au layers (white arrow). Figure 3c shows the reconstructed phase image after removing the effect. It was found that both the above-mentioned fringes completely disappeared, revealing that the effect was successfully removed and that the reconstructed phase image has only magnetic information. Although spurious signals persist in a coated Au layer due to diffraction contrast, they are negligible in the MnPd and Fe layers since the layers were epitaxially grown on the substrate. The procedure for eliminating the

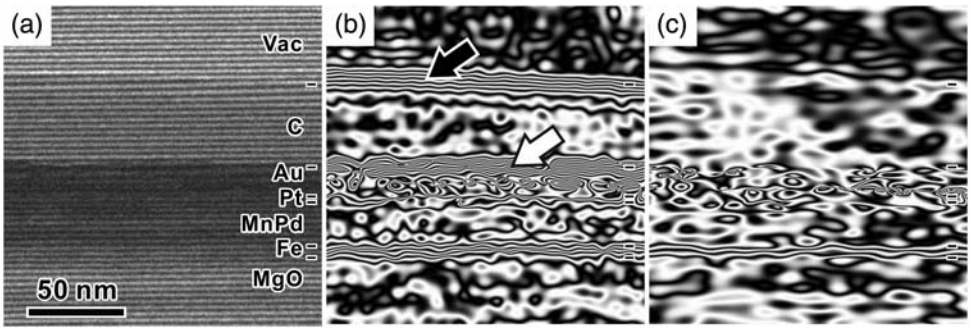

Fig. 3. (a) Electron hologram obtained from ***c*-H** and its reconstructed phase images (b) with and (c) without the effect of the mean inner potential. The layers are indicated at the right side of the images.

effect of the mean inner potential was applied to all TEM specimens.

Results and discussion

Figure 4a and b shows typical TEM images of the *c*- and *a*-oriented samples. The positions of interfaces are indicated by the white lines and the layers are labeled. The Au and C layers were coated to prevent a Ga-ion damage to the specimens during the FIB milling. The reconstructed phase images obtained from ***c*-H** (Fig. 4c), ***a*-H** (Fig. 4d), ***c*-E** (Fig. 4e) and ***a*-E** (Fig. 4f) show clear contours, parallel to the interface, in the Fe layer despite their thickness being at the limits of resolution (7 nm) of our holography system. Even though some modulations of the contours are observed, the signal is adequate for interpreting the magnetization of the Fe layers. In addition, the directions (solid arrow) of magnetization of the Fe layers, which can be estimated from a contrast gradient in reconstructed phase images presented in terms of ϕ, were well consistent with that (open arrow) of an applied magnetic field for magnetization reversal as shown in Fig. 4g.

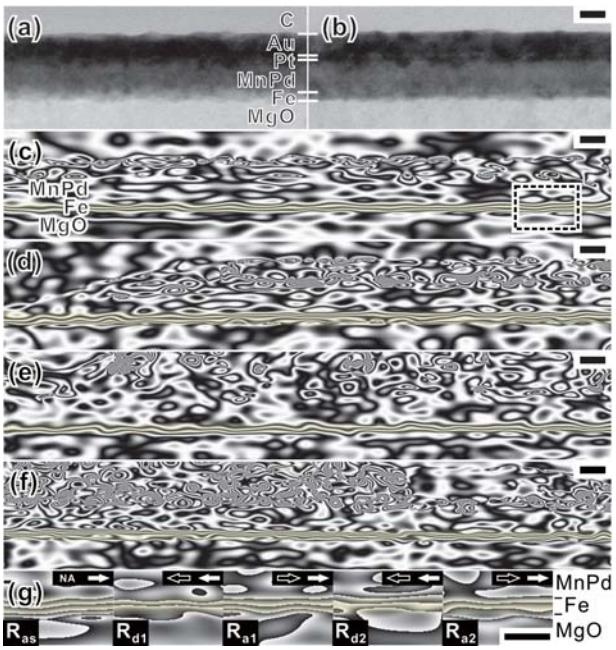

Fig. 4. Typical TEM images of (a) *c*- and (b) *a*-oriented samples; reconstructed phase images of (c) ***c*-H**, (d) ***a*-H**, (e) ***c*-E** and (f) ***a*-E**; (g) reconstructed phase images showing directions of magnetization (solid arrow) and applied external magnetic field (open arrow) at the region indicated by the dotted rectangle in (c). The reconstructed phase images are presented in terms of (c–f) cos ϕ and (g) ϕ with an amplification of 10, and scale bars = 20 nm.

Magnetic flux density (B) can be estimated from the relationship between B inside a specimen and the spacing (l) corresponding to the phase difference ($\Delta\phi$) of 2π, i.e. $B=h/etl$, where e, h and t are the elementary charge, Plank's constant and specimen thickness, respectively. In a reconstructed phase image presented in terms of cos ϕ, l is just the distance between the contour lines, i.e. white or black lines. If an amplified reconstructed phase image, where the effect of the mean inner potential is eliminated by the above-mentioned technique, is used, then the equation is modified as $B= h/2etLA$, where L is the distance between the contour lines in the reconstructed phase image which is amplified by a factor of A. The average spacing between the contour lines was determined by line profiles in the reconstructed phase image. However, to estimate B of the Fe layer, it is necessary to measure a local specimen thickness t_{Fe} at the position of the Fe layer. To measure the specimen thickness, there are several alternatives, such as convergent-beam electron diffraction [24], contamination spot-separation

[25] and EELS [26,27]. Among them, EELS can be easily applied to estimate the specimen thickness of ultra-thin layers in a multilayered sample through the 'log-ratio' formula [28], $t/\lambda_p = \ln(I_t/I_0)$, where λ_p, I_0 and I_t are, respectively, an inelastic mean free path, integrated intensity of a zero-loss peak and total integrated intensity of an EELS spectrum. Since I_0 and I_t are measured from the EELS spectrum, the specimen thickness can be simply estimated from the equation if λ_p is known. There is no literature value of λ_p for Fe at 300 kV, which is the accelerating voltage (E_0) of our TEM. Fortunately, Egerton [28] has reported λ_p for Fe as 74 nm at 100 kV with a collection semi-angle of 10 mrad. As the dependence [29] of λ_p on the acceleration voltage is $E_0^{1/2}$, the value at 300 kV can be estimated as 128 nm. Furthermore, λ_p can also be calculated from parameterized values [30] as 121 nm for 300 kV and 10 mrad. Note that the values obtained from the two different methods are close within experimental errors. Assuming $\lambda_p \sim 128$ nm, t_{Fe}'s are determined as 96, 91, 73 and 141 nm for ***c*-H**, ***a*-H**, ***c*-E** and ***a*-E**, respectively, which are reasonable for the thickness of TEM specimens prepared by FIB. The measured thicknesses might include insignificant errors regarding adopting the calculated λ_p for Fe, not the experimentally estimated one; however, the damaged layers with an amorphous phase do not affect the accuracy of the thicknesses because λ_p is insensitive to the state of a material.

B of the Fe layer at different remanence states in the four types of TEM specimens was evaluated using the equation above (Fig. 5). In descending and ascending branches of the hysteresis, the evaluated B shows some variations; however, there is no significant difference in B at between R_{d1} and R_{d2} and/or R_{a1} and R_{a2}, representing high reproducibility of the evaluation of B in this work. The averaged values of the evaluated B through all the remanence states were 0.80 ± 0.14, 1.06 ± 0.26, 1.03 ± 0.21 and 1.02 ± 0.21 T for ***c*-H**, ***a*-H**, ***c*-E** and ***a*-E**, respectively.

By comparison, interestingly, B of ***c*-H** is smaller than that of other specimens through the whole remanence states. In as-grown thin-film samples, Fe spins are aligned along their easy direction by intrinsic magnetocrystalline anisotropy of Fe [31] and are exchange coupled with MnPd spins.

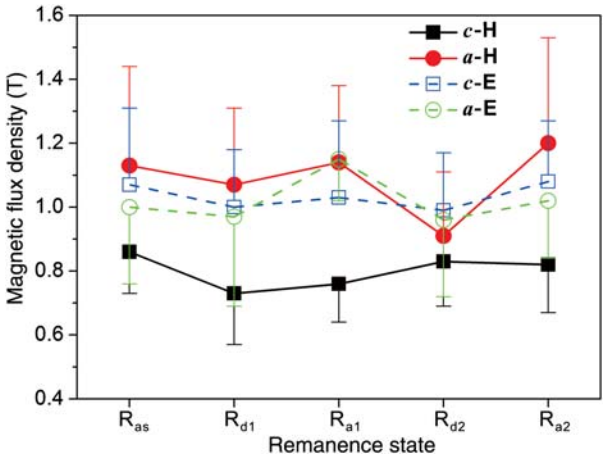

Fig. 5. Evaluated B at five different remanence states (R_{as}, R_{d1}, R_{d2}, R_{a1} and R_{a2}) for four types of TEM specimens (***c*-H**, ***a*-H**, ***c*-E** and ***a*-E**). Only half of error bars are shown.

However, in thin-foil TEM specimens with a thickness in the range of 73–141 nm studied in this work, large demagnetizing fields arise from shape anisotropies [19] due to geometry of the TEM specimen. In the case of ***c*-H** and ***a*-H**, the Fe easy axis is inclined 45° from the surface of the TEM specimen (Fig. 2a). These inclined Fe spins tend to rotate to in-plane of the TEM specimen by demagnetizing effects to suppress magnetic charges as shown in Fig. 6a, where an overall Fe spin through whole thickness is presented as the open arrow and its rotation is indicated as the angle θ. Therefore, we suggest that the spin configuration in the TEM specimens is the result of a trade-off between the strength of the spin-coupling in MnPd/Fe bilayers, the demagnetizing effects due to the shape anisotropies and the intrinsic magnetocrystalline anisotropy of Fe. It is noteworthy that the strength of the spin-coupling in MnPd/Fe bilayers is different in the *c*- and *a*-oriented samples. MOKE loops at RT indicate that the hysteresis loops in the *c*-oriented samples are more shifted as compared with the *a*-oriented samples (Fig. 7). Because a blocking temperature of the *a*-oriented samples is 90 K, the *a*-oriented samples show only a very weak EB due to a reduced long-range chemical ordering in MnPd at RT [32], whereas EB for the *c*-oriented samples, which have the blocking temperature higher than RT, is larger than that for the *a*-oriented samples. Moreover, due to low chemical ordering parameter in the *a*-oriented MnPd, the corresponding quantity of effective pinning spins is also lower as compared

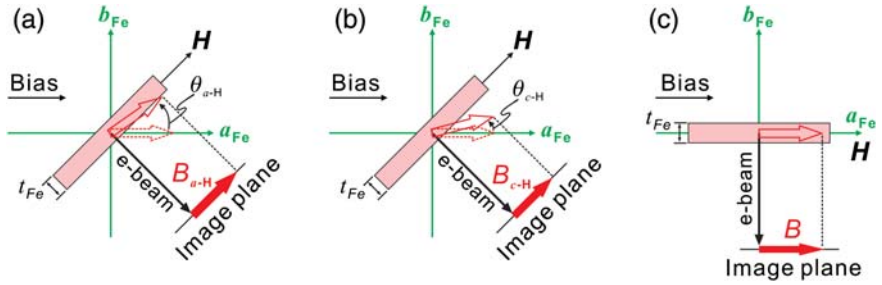

Fig. 6. Schematic illustrations for observed magnetizations in TEM specimens prepared along hard and easy axes of the Fe layer, with a side view of the specimens. Bias direction, applied field (H) direction, e-beam direction and overall Fe magnetization (open arrow) through whole thickness (t_{Fe}) and its in-plane component (B) which is measurable from the reconstructed phase image are presented.

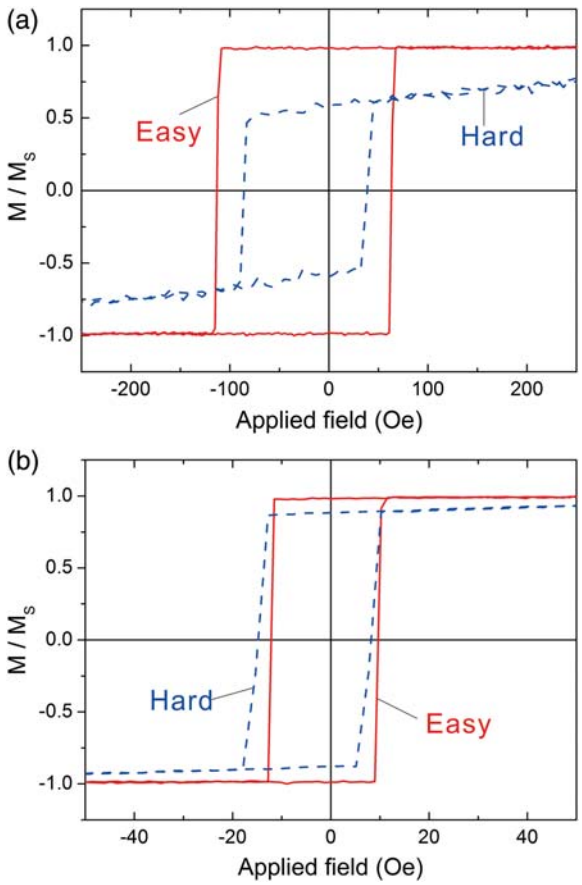

Fig. 7. MOKE loops for as-grown (a) c- and (b) a-oriented samples measured along hard and easy axes of an Fe layer.

with the c-oriented samples. From Fig. 7, the EB fields for ***c*-H** and ***c*-E** are evaluated to be –24 and –25 Oe, whereas for ***a*-H** and ***a*-E**, they are –3 and –1 Oe, meaning that the strength of the spin-coupling in the c-oriented samples is stronger than that in the a-oriented samples. Therefore, the Fe spins in ***c*-H** show more resistance against the rotation to the in-plane direction of the TEM specimen by the demagnetizing effects than that in ***a*-H**; thus, $\theta_{\boldsymbol{c}\text{-}\mathbf{H}}$ becomes smaller than $\theta_{\boldsymbol{a}\text{-}\mathbf{H}}$ as shown in Fig. 6a and b. In electron holography measurements, B obtained from a reconstructed phase image is only a component of magnetization normal to an e-beam, i.e. the in-plane component in TEM image plane [17], as shown in Fig. 6. Therefore, as θ due to the demagnetizing effects increases, B increases, and obviously, $B_{\boldsymbol{a}\text{-}\mathbf{H}}$ becomes larger than $B_{\boldsymbol{c}\text{-}\mathbf{H}}$. However, in ***c*-E** and ***a*-E**, the Fe spins were already aligned along the in-plane direction of the TEM specimen as shown in Fig. 6c; therefore, they are hardly affected by the demagnetizing effects, and ***c*-E** and ***a*-E** could have similar B values. Finally, because of a very weak spin-coupling in the a-oriented samples, it can be expected that B evaluated by electron holography is $B_{\boldsymbol{c}\text{-}\mathbf{H}} < B_{\boldsymbol{a}\text{-}\mathbf{H}} \approx B_{\boldsymbol{c}\text{-}\mathbf{E}} \approx B_{\boldsymbol{a}\text{-}\mathbf{E}}$. This interpretation is consistent with the result shown in Fig. 5 even though ***a*-H** has a little higher value than expected.

In this work, the evaluated B includes the effect of the damaged layers by the FIB milling. The damaged Fe layers consist of an amorphous phase so that the magnetic property of the damaged layers is different from that of the crystalline one. Grinstaff *et al.* [33] reported that the amorphous Fe is a soft ferromagnet. It is obvious that the damaged MnPd/Fe bilayers lose their exchange coupling and the intrinsic magnetocrystalline anisotropy of crystalline Fe disappears in the damaged layers. Therefore, the Fe spins in the damaged layers are not affected by the exchange-coupling and the intrinsic magnetocrystalline anisotropy of Fe, but only by the demagnetizing effects. It means that the magnetization in the damaged layers is not different according to the crystallographic orientation of the MnPd layers, i.e. ***a*-H** and ***c*-H**.

Consequently, even though the TEM specimens contain the damaged layers, they do not affect the tendency of B evaluated by electron holography according to the TEM specimens; they can only make a difference between the established [34] value of saturated B of pure, bulk Fe (~2.15 T) and the evaluated one.

Concluding remarks

In summary, the remanence states of exchange-biased MnPd/Fe bilayers with *c*- and *a*-oriented MnPd layers were investigated by electron holography using thin-foil TEM specimens prepared to be precisely oriented along the hard and easy axes of Fe layer. The evaluated B of the Fe layers by electron holography was 0.80 ± 0.14, 1.06 ± 0.26, 1.03 ± 0.21 and 1.02 ± 0.21 T for ***c*-H**, ***a*-H**, ***c*-E** and ***a*-E**, respectively. It is found that the spin configuration in TEM specimens originates from the trade-off between the strength of the spin-coupling at the MnPd/Fe bilayers, the shape anisotropy in the TEM specimens and the Fe magnetocrystalline anisotropy. From these results, it is believed that the electron holography can be used to investigate EB and related effects and is useful for interfacial characterization critical to further understanding of EB.

Funding

This work was supported by the Global COE Program 'Materials Integration (International Center of Education and Research), Tohoku University', MEXT, Japan, and the work at the University of Washington was supported by the US Department of Energy, Basic Energy Sciences, under contract #ER45987.

References

1 Meiklejohn W H and Bean C P (1956) New magnetic anisotropy. *Phys. Rev.* **102**: 1413–1414.

2 Tsang C (1984) Magnetics of small magnetoresistive sensors. *J. Appl. Phys.* **55**: 2226–2231.

3 Campbell I A, Hurdequint H, and Hippert F (1986) Dzyaloshinsky-Moriya anisotropy in reentrant alloys. *Phys. Rev. B* **33**: 3540–3542.

4 Nogués J, Moran T J, Lederman D, Schuller I K, and Rao K V (1999) Role of interfacial structure on exchange-biased FeF_2–Fe. *Phys. Rev. B* **59**: 6984–6993.

5 Nogués J and Schuller I K (1999) Exchange bias. *J. Magn. Magn. Mater.* **192**: 203–232.

6 Krishnan K M, Pakhomov A B, Bao Y, Blomqvist P, Chun Y, Gonzales M, Griffin K, Ji X, and Roberts B K (2006) Nanomagnetism and spin electronics: materials, microstructure and novel properties. *J. Mater. Sci.* **41**: 793–815.

7 Blomqvist P, Krishnan K M, and Ohldag H (2005) Direct imaging of asymmetric magnetization reversal in exchange-biased Fe/MnPd bilayers by X-ray photoemission electron microscopy. *Phys. Rev. Lett.* **94**: 107203.

8 Srajer G, Lewis L H, Bader S D, Epstein A J, Fadley C S, Fullerton E E, Hoffmann A, Kortright J B, Krishnan K M, Majetich S A, Rahman T S, Ross C A, Salamon M B, Schuller I K, Schulthess T C, and Sun J Z (2006) Advances in nanomagnetism via X-ray techniques. *J. Magn. Magn. Mater.* **307**: 1–31.

9 Malozemoff A P (1987) Random-field model of exchange anisotropy at rough ferromagnetic–antiferromagnetic interfaces. *Phys. Rev. B* **35**: 3679–3682.

10 Takano K, Kodama R H, Berkowitz A E, Cao W, and Thomas G (1997) Interfacial uncompensated antiferromagnetic spins: role in unidirectional anisotropy in polycrystalline $Ni_{81}Fe_{19}$/CoO bilayers. *Phys. Rev. Lett.* **79**: 1130.

11 Koon N C (1997) Calculations of exchange bias in thin films with ferromagnetic/antiferromagnetic interfaces. *Phys. Rev. Lett.* **78**: 4865–4868.

12 Mauri D, Siegmann H C, Bagus P S, and Kay E (1987) Simple model for thin ferromagnetic films exchange coupled to an antiferromagnetic substrate. *J. Appl. Phys.* **62**: 3047–3049.

13 Kiwi M, Mejía-López J, Portugal R D, and Ramirez R (1999) Exchange-bias systems with compensated interfaces. *Appl. Phys. Lett.* **75**: 3995–3997.

14 Tang L, Laughlin D E, and Gangopadhyay S (1997) Microstructural study of ion-beam deposited giant magnetoresistive spin valves. *J. Appl. Phys.* **81**: 4906–4908.

15 Krishnan K M, Nelson C, Echer C J, Farrow R F C, Marks R F, and Kellock A J (1998) Exchange biasing of permalloy films by Mn_xPt_{1-x}: role of composition and microstructure. *J. Appl. Phys.* **83**: 6810–6812.

16 Portier X, Petford-Long A K, Anthony T C, and Brug J A (1999) Temperature dependence of the reversal mechanism in spin-valve films. *Appl. Phys. Lett.* **75**: 1290–1292.

17 Shindo D and Oikawa T (2002) *Analytical Electron Microscopy for Materials Science* (Springer, Tokyo).

18 Dunin-Borkowski R E, Mccartney M R, Kardynal B, Scheinfein M R, Smith D J, and Parkin S S P (2001) Off-axis electron holography of exchange-biased CoFe/FeMn patterned nanostructures. *J. Appl. Phys.* **90**: 2899–2902.

19 Leslie-Pelecky D L and Rieke R D (1996) Magnetic properties of nanostructured materials. *Chem. Mater.* **8**: 1770–1783.

20 Cheng N, Ahn J, and Krishnan K M (2001) Epitaxial growth and exchange biasing of PdMn/Fe bilayers grown by ion-beam sputtering. *J. Appl. Phys.* **89**: 6597–6599.

21 Blomqvist P, Krishnan K M, and Mccready D E (2004) Growth of exchange-biased MnPd/Fe bilayers. *J. Appl. Phys.* **95**: 8019–8022.

22 Pál L, Krén E, Kádár G, Szabó P, and Tarnóczi T (1968) Magnetic structures and phase transformations in Mn-based CuAu-I type alloys. *J. Appl. Phys.* **39**: 538–544.

23 Tonomura A, Matsuda T, Endo J, Arii T, and Mihama K (1986) Holographic interference electron microscopy for determining specimen magnetic-structure and thickness distribution. *Phys. Rev. B* **34**: 3397–3402.

24 Allen S M and Hall E L (1982) Foil thickness measurements from convergent-beam diffraction patterns – an experimental assessment of errors. *Phil. Mag. A* **46**: 243–253.

25 Hirsch P B, Howie A, Nicholson R B, Pashley D W, and Whelan M J (1977) *Electron Microscopy of Thin Crystals*, 2nd edn. (Krieger, New York).

26 Leapman R D, Fiori C E, and Swyt C R (1984) Mass thickness determination by inelastic scattering in microanalysis of organic samples. In: Williams D B and Joy D C (eds), *Analytical Electron Microscopy* (San Francisco Press, San Francisco).

27 Lee C W, Ikematsu Y, and Shindo D (2000) Thickness measurement of amorphous SiO_2 by EELS and electron holography. *Mater. Trans. JIM* **41**: 1129–1131.

28 Egerton R F (1996) *Electron Energy-Loss Spectroscopy in the Electron Microscope*, 2nd edn. (Plenum Press, New York).

29 Grimm R, Typke D, Bärmann M, and Baumeister W (1996) Determination of the inelastic mean free path in ice by examination of tilted vesicles and automated most probable loss imaging. *Ultramicroscopy* **63**: 169–179.

30 Malis T, Cheng S C, and Egerton R F (1988) EELS log-ratio technique for specimen-thickness measurement in the TEM. *J. Electron Microsc. Technol.* **8**: 193–200.

31 Zhan Q F and Krishnan K M (2010) Angular dependence of magnetization reversal process in exchange biased epitaxial MnPd/Fe bilayers. *J. Appl. Phys.* **107**: 09D703.

32 Zhan Q F and Krishnan K M (2010) In-plane reorientation of magnetization in epitaxial exchange biased Fe/MnPd bilayers. *Appl. Phys. Lett.* **96**: 112506.

33 Grinstaff M W, Salamon M B, and Suslick K S (1993) Magnetic properties of amorphous iron. *Phys. Rev. B* **48**: 269–273.

34 Ida N (2004) *Engineering Electromagnetic*, 2nd edn. (Springer, New York).